**Cell Reports Medicine, Volume *1***

## Supplemental Information

# Targeting Mitochondrial Complex I Overcomes Chemoresistance in High OXPHOS Pancreatic Cancer

**Rawand Masoud, Gabriela Reyes-Castellanos, Sophie Lac, Julie Garcia, Samir Dou, Laetitia Shintu, Nadine Abdel Hadi, Tristan Gicquel, Abdessamad El Kaoutari, Binta Diémé, Fabrice Tranchida, Laurie Cormareche, Laurence Borge, Odile Gayet, Eddy Pasquier, Nelson Dusetti, Juan Iovanna, and Alice Carrier**

# SUPPLEMENTAL INFORMATION

# Targeting mitochondrial Complex I overcomes chemoresistance in high OXPHOS pancreatic cancer

Rawand Masoud[1]†*, Gabriela Reyes-Castellanos[1]†, Sophie Lac[1]‡, Julie Garcia[1], Samir Dou[1], Laetitia Shintu[2], Nadine Abdel Hadi[1], Tristan Gicquel[1], Abdessamad El Kaoutari[1], Binta Diémé[2]§, Fabrice Tranchida[2], Laurie Cormareche[1], Laurence Borge[1], Odile Gayet[1], Eddy Pasquier[1], Nelson Dusetti[1], Juan Iovanna[1], Alice Carrier[1]*#

**Affiliations:**

[1]Aix Marseille Université, CNRS, INSERM, Institut Paoli-Calmettes, Centre de Recherche en Cancérologie de Marseille (CRCM), F-13009 Marseille, France.

[2]Aix Marseille Université, CNRS, Centrale Marseille, ISM2, F-13013 Marseille, France

*To whom correspondence should be addressed: Alice Carrier and Rawand Masoud, Centre de Recherche en Cancérologie de Marseille (CRCM), Campus de Luminy Case 915, 163 Avenue de Luminy, 13288 Marseille Cedex 9, France. Phone : +33 491828829 ; Fax : +33 491826083. Email: alice.carrier@inserm.fr and rawand.masoud@inserm.fr.

† These authors contributed equally

‡ Current address: Innate Pharma, F-13009 Marseille

§ Current address: Institut de Chimie de Clermont-Ferrand, PlateForme d'Exploration du Métabolisme (PFEM), Université Clermont-Auvergne, F-63000 Clermont-Ferrand, France

# Lead contact

**List of supplementary data:**

Supplementary Figures: 9

Supplementary Tables: 2

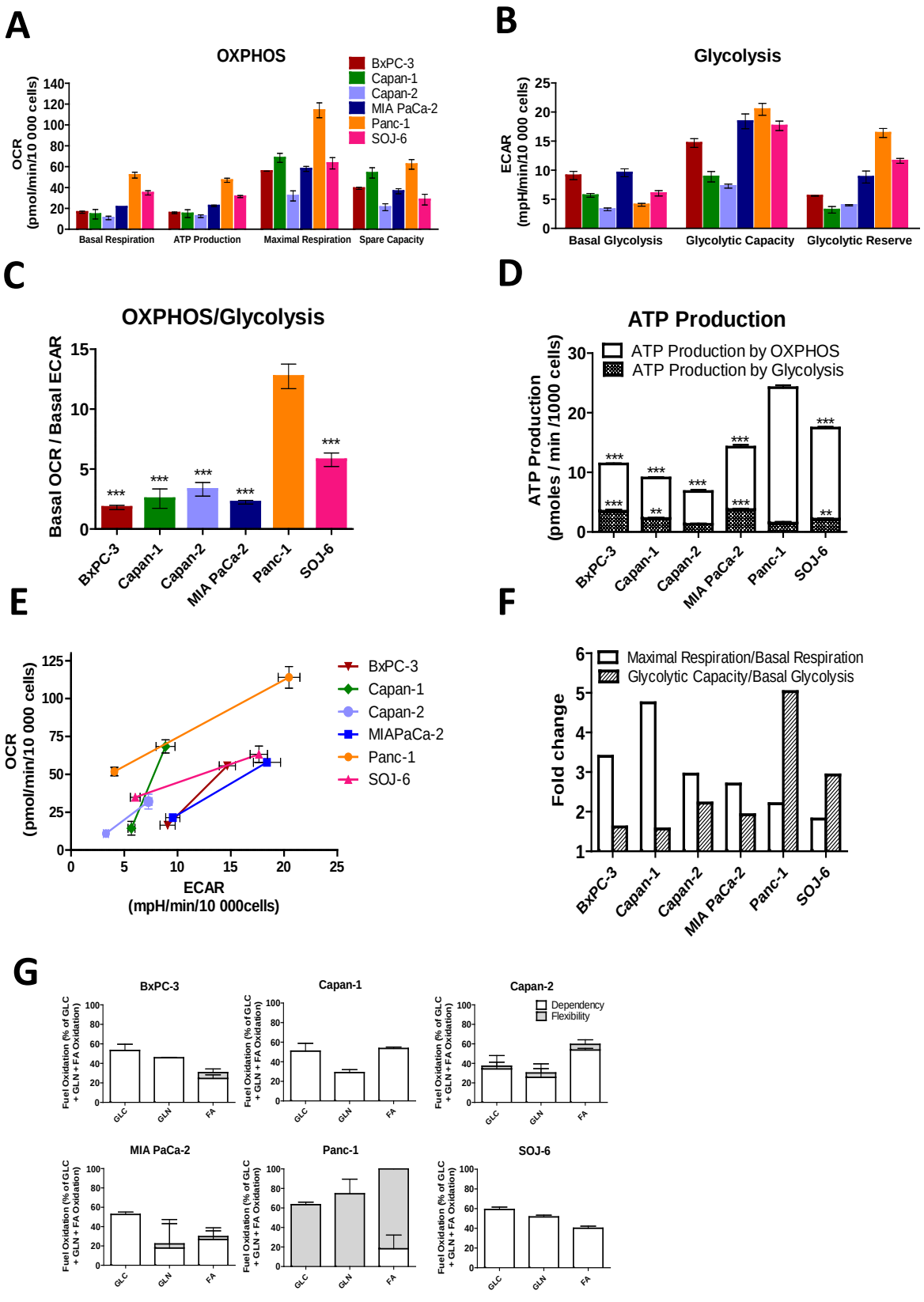
A
OXPHOS
OCR (pmol/min/10 000 cells)
BxPC-3
Capan-1
Capan-2
MIA PaCa-2
Panc-1
SOJ-6
Basal Respiration
ATP Production
Maximal Respiration
Spare Capacity
B
Glycolysis
ECAR (mpH/min/10 000 cells)
Basal Glycolysis
Glycolytic Capacity
Glycolytic Reserve
C
OXPHOS/Glycolysis
Basal OCR / Basal ECAR
D
ATP Production
ATP Production (pmoles / min /1000 cells)
ATP Production by OXPHOS
ATP Production by Glycolysis
E
OCR (pmol/min/10 000 cells)
ECAR (mpH/min/10 000cells)
MIAPaCa-2
F
Fold change
Maximal Respiration/Basal Respiration
Glycolytic Capacity/Basal Glycolysis
G
Fuel Oxidation (% of GLC + GLN + FA Oxidation)
GLC
GLN
FA
Dependency
Flexibility

**Supplementary Figure 1. Mitochondrial metabolism is efficient in pancreatic cancer cells (related to Figure 1A - C).** (**A, B**) Quantification of representative profiles obtained for OXPHOS (**A**) and glycolysis (**B**) experiments for the six classical PDAC cell lines. (**A**) The rates of OCR (mean of triplicates ± SEM) for basal respiration, mitochondrial ATP production, maximal respiration and spare capacity were quantified as described in the Materials and Methods section, and normalized to 10,000 seeded cells. This graph is representative of at least three independent experiments. (**B**) The rates of ECAR (mean of triplicates ± SEM) for glycolysis, glycolytic capacity, and glycolytic reserve were quantified as described in the Materials and Methods section, and normalized to 10,000 seeded cells. This graph is representative of at least three independent experiments. (**C**) Ratio of basal OCR to basal ECAR. Statistically significant differences between Panc-1 cells with the 5 others *** $p<0.001$. (**D**) ATP production by OXPHOS and glycolysis was determined by the OCR and proton production rate, respectively. Statistically significant differences between the Panc-1 cell line with the 5 other cell lines: ** and *** $p<0.01$ and $p<0.001$ respectively. (**E-F**) Two different representations of cell metabolic plasticity. (**E**) OCR versus ECAR plot showing for each cell line basal OCR and ECAR linked by a line with maximal OCR and ECAR. (**F**) Fold change levels of maximal respiration to basal respiration and fold change levels of glycolytic capacity to basal glycolysis were determined for each PDAC cell line. (**G**) Pancreatic cancer cells demonstrate different degrees of dependency and flexibility towards essential TCA fuels. OCR was measured when cells were challenged with fuel pathway inhibitors: UK5099, BPTES, and Etomoxir, targeting Glucose (GLC), Glutamine (GLN), and Fatty Acids (FA) pathways, respectively. The dependency and flexibility of cells to oxidize these three critical mitochondrial fuels were determined as described in the Supplementary Materials and Methods section. Data are presented as the mean of triplicates ± SEM. Data are representative of three independent experiments.

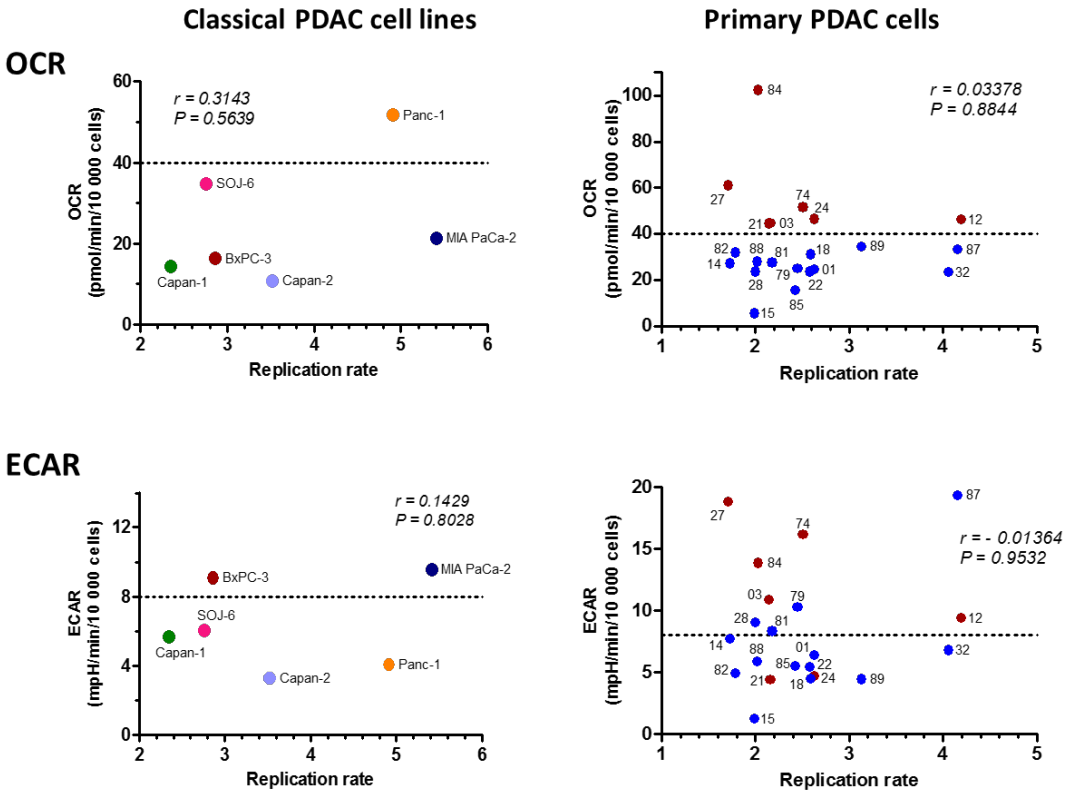


**Supplementary Figure 2. The metabolic status of PDAC cells is unrelated to their proliferation rate (related to Figure 1).** The replication rate in 72 hours was monitored by PrestoBlue labelling of cells seeded in 96-well plate the day after the seeding (D0) and 3 days later (D3), as described in Gayet *et al*., 2015. The scatterplots display the replication rate and the corresponding basal OCR or basal ECAR, of both classical PDAC cell lines (left) and the 21 primary PDAC cells (right). High and low OXPHOS primary PDAC cells are in red and blue dots, respectively, and identified with a short version of the anonymized name of patients. The horizontal dotted line indicates the threshold that we selected in Figure 1C and D between high and low OCR or ECAR. Spearman's correlation coefficient and p values are shown, indicating none or very weak association between the two variables, with non-statistically significant values in any of the cases.

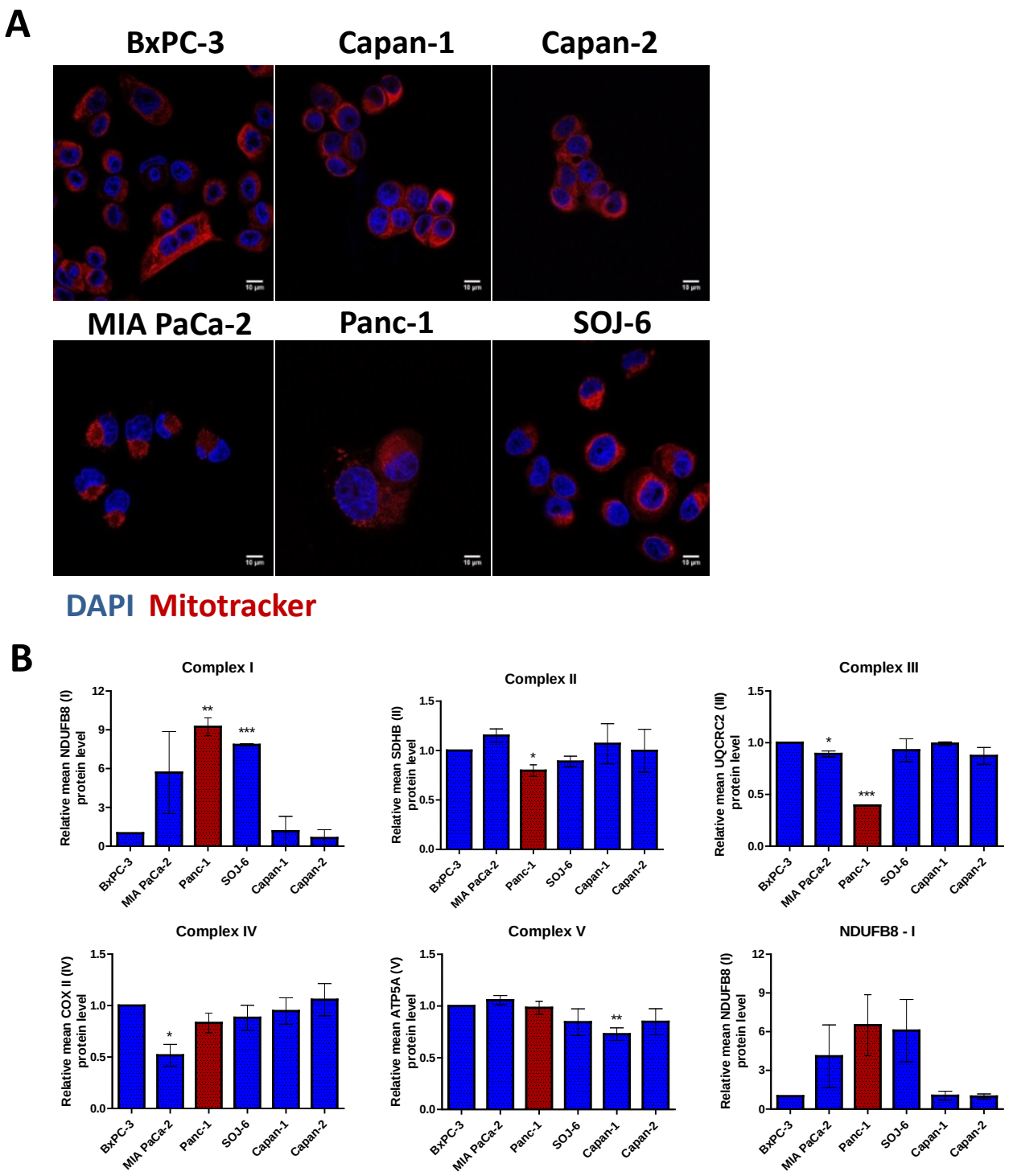


**Supplementary Figure 3. Abundance of respiratory Complex I reflects respiration activity (related to Figure 2A - F).** (**A**) Representative confocal microscopy images of stained cells with MitoTracker DeepRed (red) and DAPI (blue) are shown. (**B**) Mitochondrial complexes protein levels were quantified on WB by Image J, normalized to BxPC-3 cell line, and the mean of 3 different WB was calculated (*, ** and *** $p<0.05$, $p<0.01$ and $p<0.001$ respectively). The last graph (NDUFB8-I) corresponds to the Western blot using the anti-NDUFB8 antibody alone.

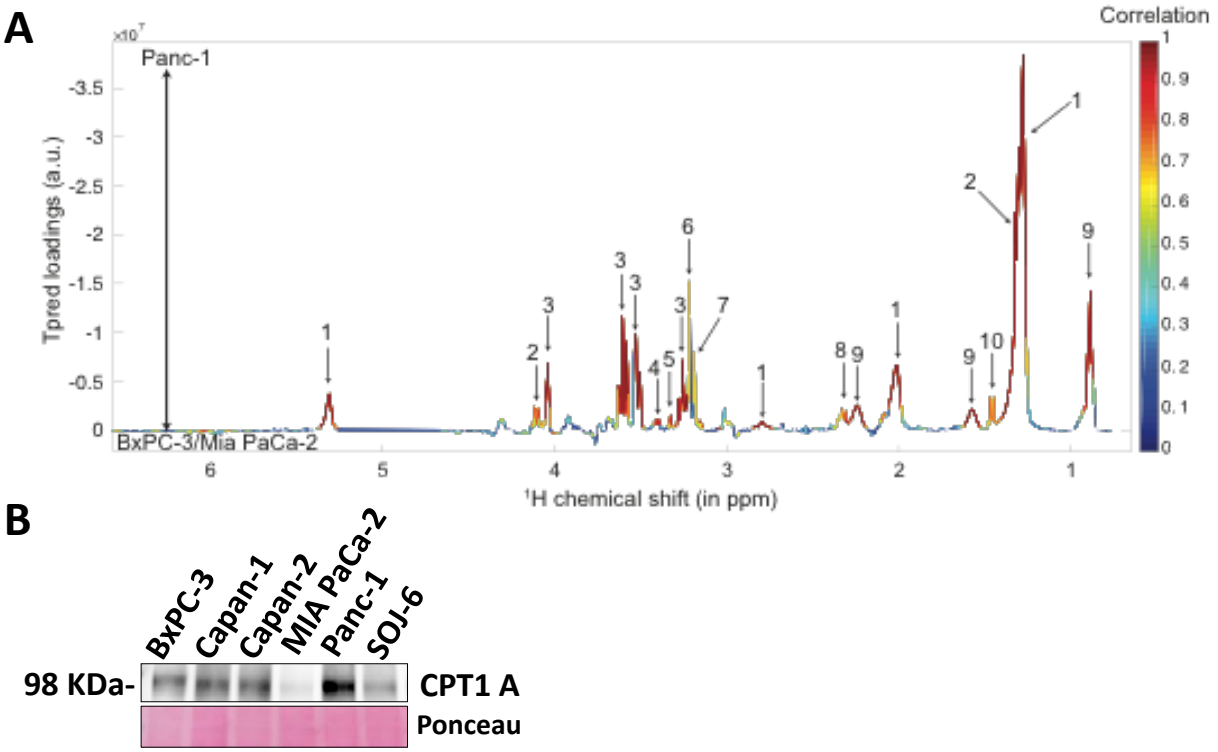


**Supplementary Figure 4. High OXPHOS Panc-1 cells show metabolic specificities (related to Figure 2G).** (**A**) Representative profile of metabolic analysis by HRMAS-NMR. OPLSDA predictive component loading plot showing the weights of each NMR variable in the discrimination in OXPHOS Panc-1 cells (Top part) versus glycolytic BxPC-3/ MIA PaCa-2 cells (Bottom part). The NMR variables are color-coded according to their correlation coefficients with the predictive component. Significantly discriminant metabolites were annotated on the loading plot. 1: unsaturated fatty acids; 2: lactate; 3: myo-inositol; 4: proline/taurine; 5: scyllo-inositol; 6: glycerophosphocholine/phosphocholine; 7: choline; 8: glutamate; 9: fatty acids; 10: alanine. (**B**) CPT1A Western blotting for the classical PDAC cell lines. Ponceau coloration is shown as control of equal protein loading.

**A**

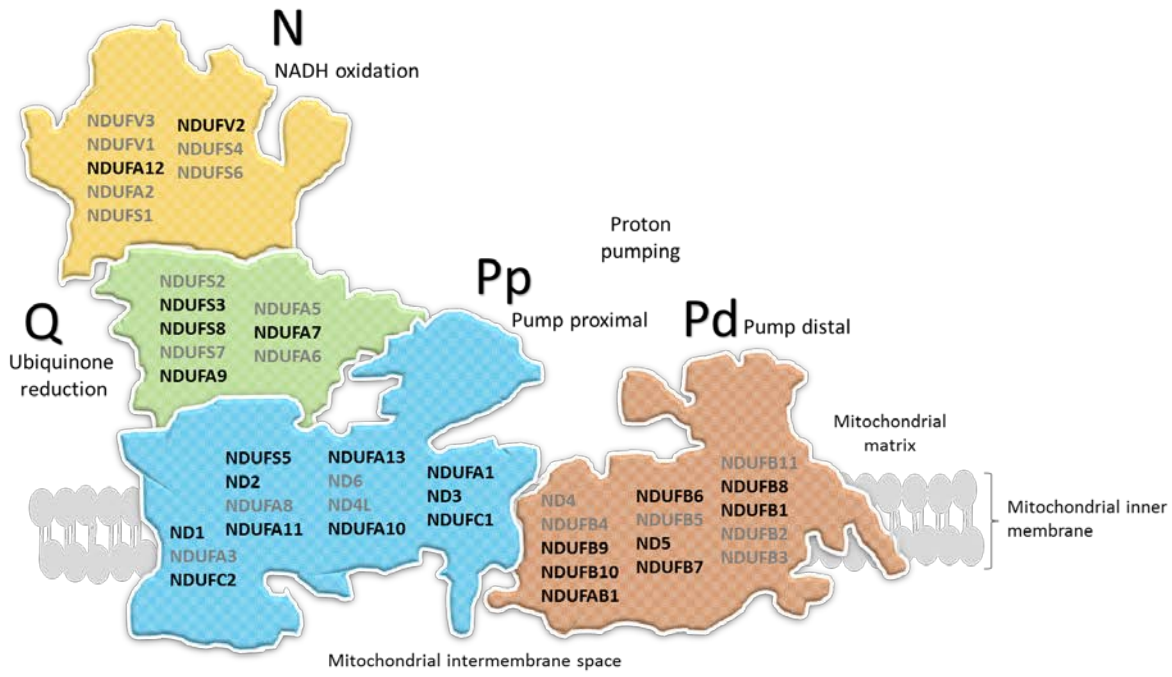
N
NADH oxidation
NDUFV3
NDUFV1
NDUFA12
NDUFA2
NDUFS1
NDUFV2
NDUFS4
NDUFS6
Proton pumping
Pp
Pump proximal
Pd
Pump distal
Q
Ubiquinone reduction
NDUFS2
NDUFS3
NDUFS8
NDUFS7
NDUFA9
NDUFA5
NDUFA7
NDUFA6
Mitochondrial matrix
NDUFS5
ND2
NDUFA8
ND1
NDUFA3
NDUFC2
NDUFA11
NDUFA13
ND6
ND4L
NDUFA10
NDUFA1
ND3
NDUFC1
ND4
NDUFB4
NDUFB9
NDUFB10
NDUFAB1
NDUFB6
NDUFB5
ND5
NDUFB7
NDUFB11
NDUFB8
NDUFB1
NDUFB2
NDUFB3
Mitochondrial inner membrane
Mitochondrial intermembrane space

**B**

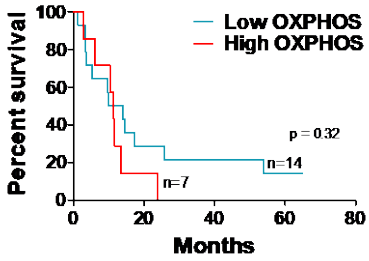
Low OXPHOS
High OXPHOS
Percent survival
100
80
60
40
20
0
0
20
40
60
80
Months
p = 0.32
n=14
n=7

**C**

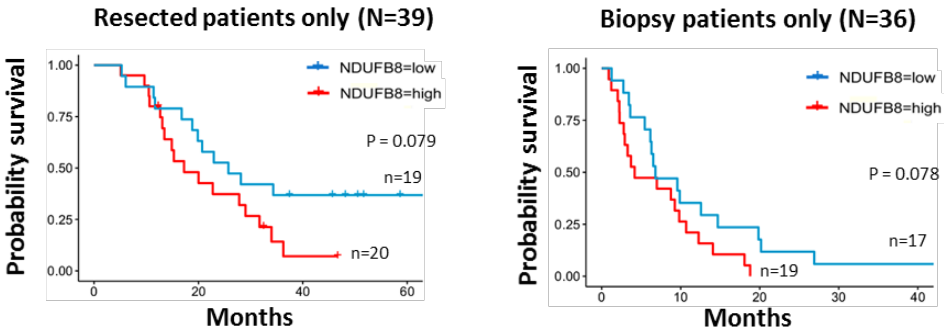
Resected patients only (N=39)
Probability survival
1.00
0.75
0.50
0.25
0.00
0
20
40
60
Months
NDUFB8=low
NDUFB8=high
P = 0.079
n=19
n=20
Biopsy patients only (N=36)
Probability survival
1.00
0.75
0.50
0.25
0.00
0
10
20
30
40
Months
NDUFB8=low
NDUFB8=high
P = 0.078
n=17
n=19

**Supplementary Figure 5. Enrichment of mitochondrial respiratory chain Complex I in high OXPHOS PDAC patients (related to Figure 3 and Supplementary Table 2).** (**A**) Schematic overview of the mammalian mitochondrial Complex I composed of 4 functional modules and 44 subunits, inspired by the review of Giachin *et al*. 2016 (Giachin G. Front Mol Biosci 2016, 3:43). The 24 Complex I-subunits genes that were found enriched in the high OXPHOS compared to low OXPHOS PDAC patients are represented in black font. (**B**) Kaplan-Meier survival curve for high and low OXPHOS patient groups (n=7 and n=14, respectively). p value was calculated by the log-rank (Mantel-Cox) statistic test. (**C**) Kaplan-Meier survival curves using transcriptomic analysis on patient-derived xenografts, divided into high and low NDUFB8 subunit expression (cutpoint 13.22) for PDAC patients with resectable tumors (left; n = 39) and biopsy patients only (right; n = 36). p values from the log-rank statistic test.

**A**

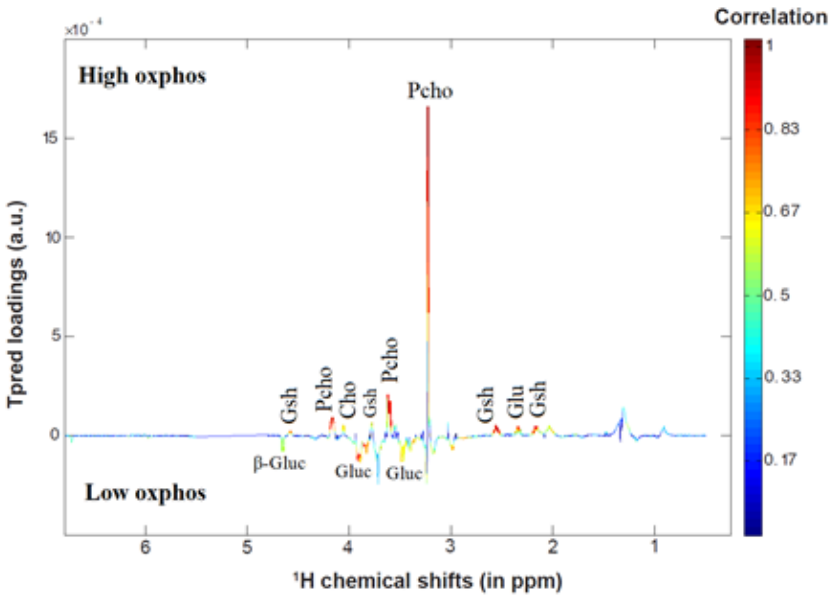


**B**

| **Metabolites** | **$^1$H chemical shift (in ppm), multiplicity and assignment** | **High oxphos/ Low oxphos[a]** | **P-value** |
|---|---|---|---|
| Choline | 3.21 (s) $CH_3$, **4.05** (m) $CH_2$ | 1.97 | <0.001 |
| Phosphocholine | **3.22** (s) $CH_3$, 3.59 (m) $CH_2$, 4.16 (m) $CH_2$ | 5.31 | <0.001 |
| Glucose | 4.64 (d) CH, **3.90**, 3.83, 3.47, 3.40 unresolved signals | 0.52 | <0.001 |
| Glutamate | **2.34** (m) $\gamma CH_2$, 2.04 (m) $\beta CH_2$, 2.11 (m) $\beta CH_2$ | 1.63 | <0.001 |
| Glutathione | 4.58 (m) CH, 3.77 (m) CH, **2.56** (m) $CH_2$, 2.17 (m) $CH_2$ | 2.68 | <0.001 |
| Unknown | **2.98,** 1.66, 1.44 broad | 0.55 | <0.001 |

s = singlet; d = doublet; m = multiplet

**Supplementary Figure 6. High OXPHOS PDAC cells show metabolic specificities compared to low OXPHOS (related to Figure 3E).** (**A**) Representative profile of metabolic analysis by HRMAS-NMR of primary cells from 3 High OXPHOS PDAC patients versus 3 low OXPHOS. OPLSDA predictive component loading plot showing the weights of each NMR variable in the discrimination in High OXPHOS (Top part) versus Low OXPHOS (Bottom part). The NMR variables are color-coded according to their correlation coefficients with the predictive component. Significantly discriminant metabolites were annotated on the loading plot. Abbreviations : Cho = choline, Glu = glutamate, Gluc = Glucose, Gsh = Glutathione, Pcho = Phosphocholine. (**B**) Metabolites that contributed significantly to the discrimination between the High OXPHOS and Low OXPHOS in the OPLS-DA model from the $^1$H NMR data. [a]Fold change in metabolite level followed by P-value (t-test).

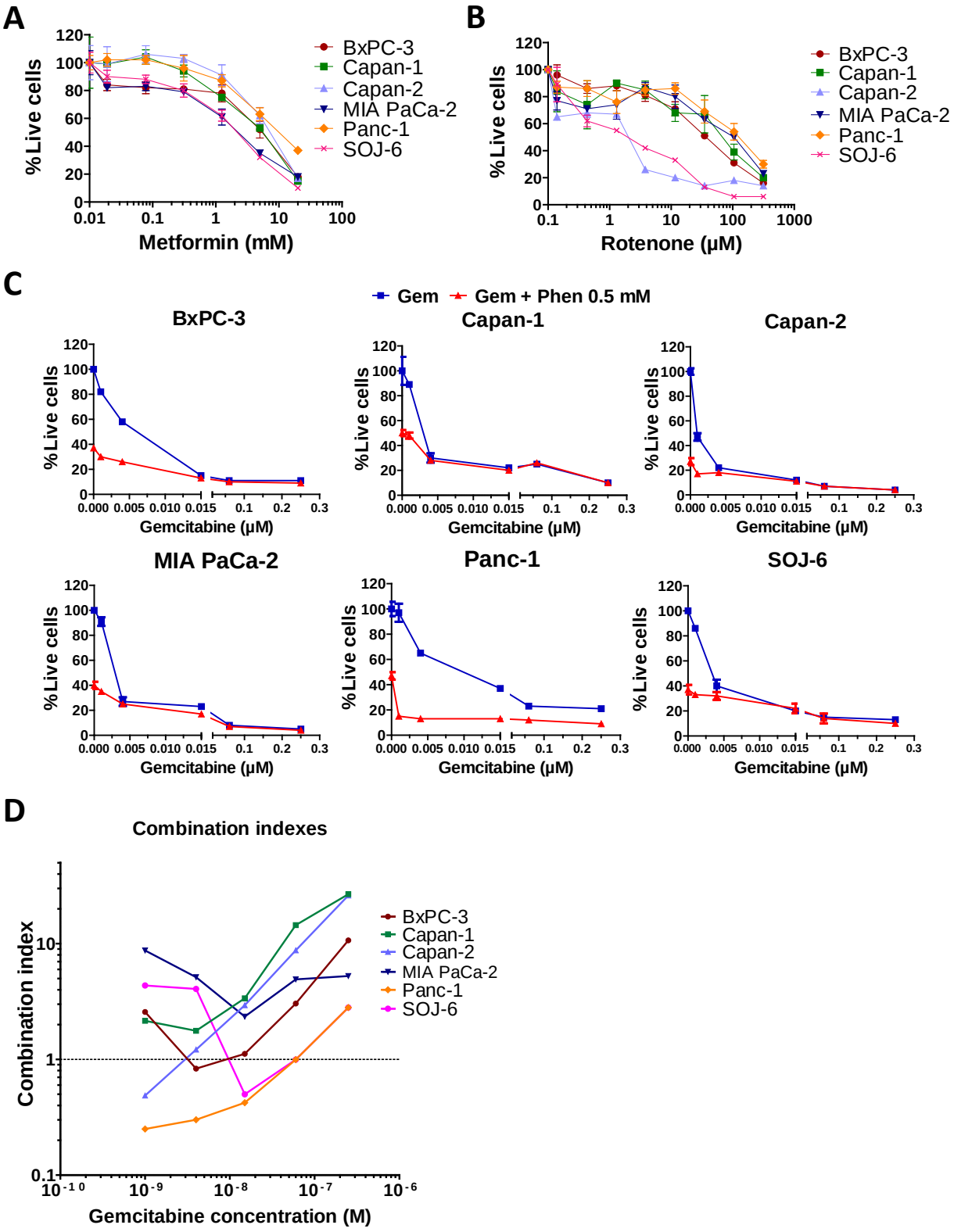
A
% Live cells
Metformin (mM)
BxPC-3
Capan-1
Capan-2
MIA PaCa-2
Panc-1
SOJ-6
B
% Live cells
Rotenone (μM)
C
Gem
Gem + Phen 0.5 mM
BxPC-3
Capan-1
Capan-2
MIA PaCa-2
Panc-1
SOJ-6
Gemcitabine (μM)
D
Combination indexes
Combination index
Gemcitabine concentration (M)

**Supplementary Figure 7. Classical PDAC cells are sensitive to drugs targeting mitochondrial respiratory Complex I, and Phenformin synergizes with Gemcitabine in high OXPHOS PDAC cells (related to Figure 4A - C).** (**A-B**) Dose-response curves to treatment of the six classical PDAC cell lines with Metformin and Rotenone, respectively. Live cells are indicated as a % of the control (vehicle treated). Data are means of triplicates ± SEM. (**C**) Representative dose-response curves for the six PDAC cell lines treated with different concentrations of Gemcitabine alone (blue curves) and Gemcitabine in combination with 0.5 mM Phenformin (red curves) for 72h. Cell viability is indicated as a % of the control (vehicle treated). Data are means of triplicates ± SEM. (**D**) Combination indexes (CI) for Phenformin 0.5 mM treatment with Gemcitabine at different concentrations, according to the Chou and Talalay method: additive effects ($0.8 \leq CI \leq 1.2$), synergism ($CI < 0.8$) and antagonism ($CI > 1.2$) in drug combinations.

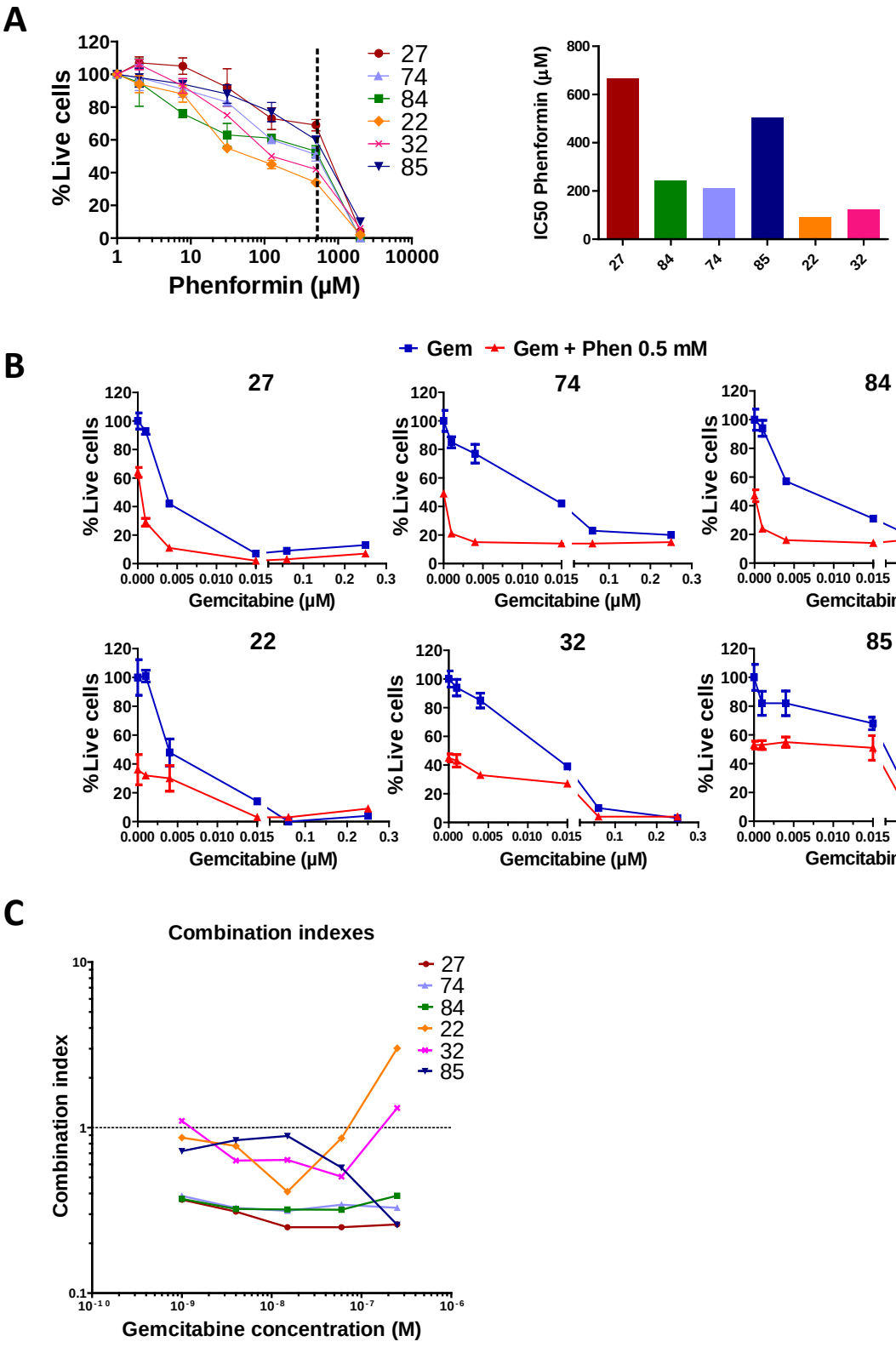
A
% Live cells
Phenformin (μM)
27
74
84
22
32
85
IC50 Phenformin (μM)
B
Gem
Gem + Phen 0.5 mM
Gemcitabine (μM)
C
Combination indexes
Combination index
Gemcitabine concentration (M)

**Supplementary Figure 8. Phenformin treatment synergizes with Gemcitabine in high OXPHOS primary PDAC cells (related to Figure 4D).** (**A**) Dose-response curve to Phenformin treatment (left) of six primary PDAC cells: 3 high OXPHOS patients (27, 74, and 84) and 3 low OXPHOS (22, 32, and 85). Live cells are indicated as a % of the control (vehicle treated). Data are means of triplicates ± SEM. The IC50 values of Phenformin (Right) were calculated from the dose-response curve. (**B**) Representative dose-response curves of the six primary PDAC cells treated with different concentrations of Gemcitabine alone (blue curves) and Gemcitabine in combination with 0.5 mM Phenformin (red curves) for 72h. Cell viability is indicated as a % of the control (vehicle treated). Data are means of triplicates ± SEM. (**C**) Combination indexes (CI) for Phenformin 0.5 mM treatment with Gemcitabine at different concentrations, according to the Chou and Talalay method. Combination treatment specifically sensitizes high OXPHOS cells (27, 74, and 84) to Gemcitabine, with combination indexes lower than 0.5 that means strong synergy.

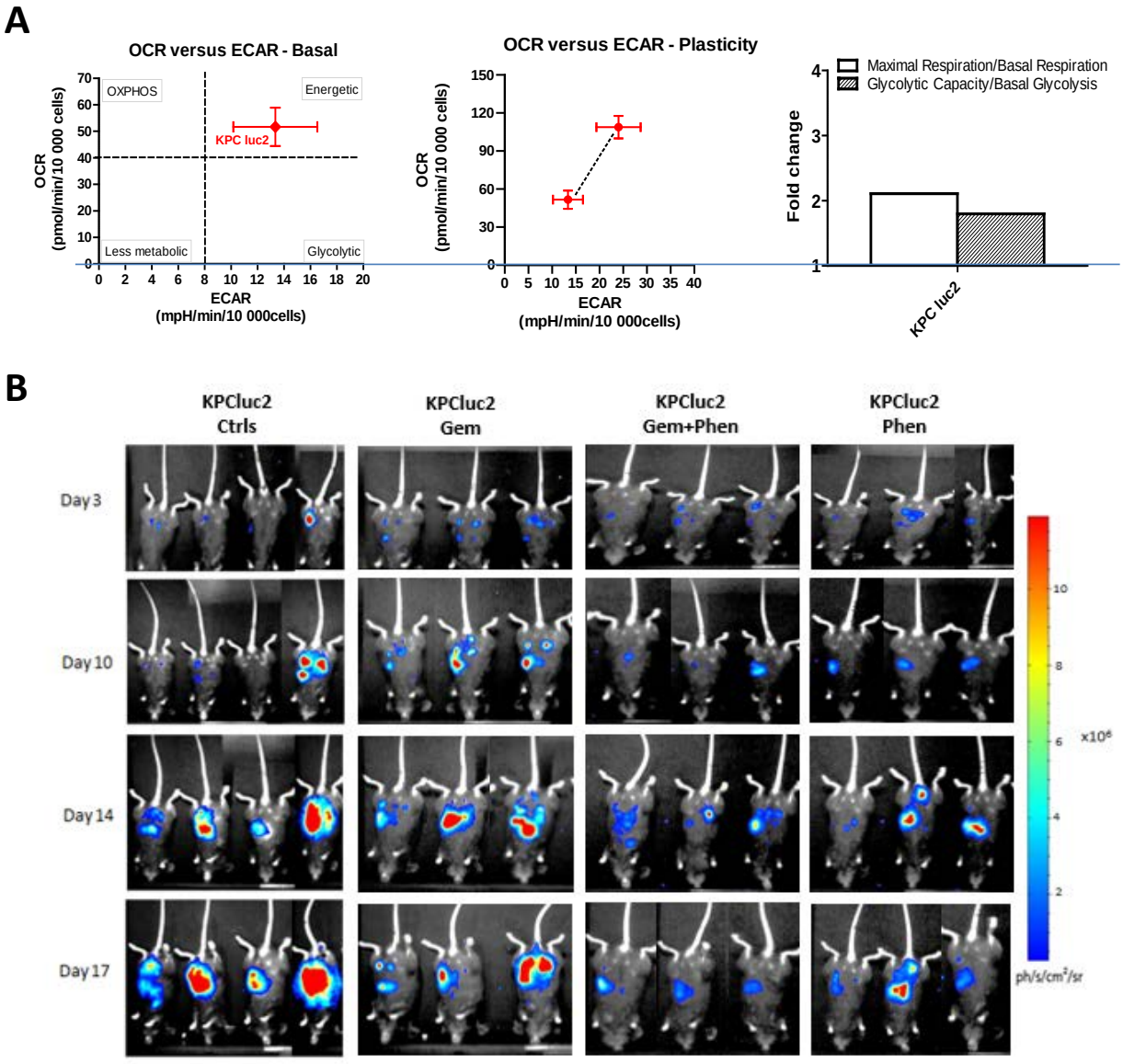

**Supplementary Figure 9. Phenformin enhances Gemcitabine antitumoral activity in high OXPHOS murine PDAC cells (related to Figure 6D and E).** (**A**) Seahorse data. Left: basal OCR versus basal ECAR plot. Middle and Right: two different representations of cell metabolic plasticity, as described in the legend of Supplementary Figure 1E-F. The data are representative of 6 independent experiments (**B**) Representative *in vivo* bioluminescence imaging data at different times after orthotopic implantation of KPC luc2 cells.

**Supplementary Table 1 (related to Figure 1 and S9A).** Cell density and FCCP concentration used in Seahorse experiments, and KRAS and p53 genetic status for each PDAC cell line: 6 classical human cell lines, 21 from patients of the PaCaOmics cohort for which the name was anonymized, and the murine KPC luc2 cell line. The genetic information for the PaCaOmics patients is available in Nicolle R. *et al*., 2017. NA = not available. All PaCaOmics tumors are KRAS mutated except one (PDAC012T) and all PaCaOmics tumors for which the p53 status was investigated (12 over 21) are mutated or lost except one (PDAC032T).

| Cell line | Cellular density | [FCCP] µM | KRAS status | p53 mutated/loss |
|---|---|---|---|---|
| **BxPC-3** | 40 000 | 0.25 | WT | Mut |
| **Capan-1** | 40 000 | 0.5 | Mut | Mut |
| **Capan-2** | 40 000 | 0.25 | Mut | WT |
| **MIA PaCa-2** | 40 000 | 0.125 | Mut | Mut |
| **Panc-1** | 40 000 | 0.5 | Mut | Mut |
| **SOJ-6** | 40 000 | 0.25 | Unknown | Unknown |
| **PDAC001T** | 30 000 | 0.5 | G12D (homo) | Mut |
| **PDAC003T** | 30 000 | 0.5 | G12D (hetero) | Mut/loss |
| **PDAC012T** | 50 000 | 0.5 | 12-13 WT | Mut/loss |
| **PDAC014T** | 40 000 | 0.5 | G12V (hetero) | Mut/loss |
| **PDAC015T** | 20 000 | 1 | G12D (hetero) | Mut/loss |
| **PDAC018T** | 15 000 | 1 | G12D (hetero) | Mut/loss |
| **PDAC021T** | 30 000 | 0.5 | G12V (hetero) | Mut/loss |
| **PDAC022T** | 40 000 | 1 | G12R (hetero) | Mut/loss |
| **PDAC024T** | 30 000 | 0.5 | G12D (homo) | Mut/loss |
| **PDAC027T** | 20 000 | 0.5 | G12V (hetero) | Mut/loss |
| **PDAC028T** | 40 000 | 0.5 | G12V (homo) | Mut/loss |
| **PDAC032T** | 40 000 | 1 | G12D (hetero) | WT |
| **PDAC074T** | 20 000 | 0.25 | G12D (hetero) | NA |
| **PDAC079T** | 30 000 | 0.5 | G12D (homo) | NA |
| **PDAC081T** | 40 000 | 0.5 | G12D (hetero) | NA |
| **PDAC082T** | 30 000 | 1 | G12V (hetero) | NA |
| **PDAC084T** | 20 000 | 0.5 | G12V (hetero) | NA |
| **PDAC085T** | 40 000 | 0.5 | G12V (hetero) | NA |
| **PDAC087T** | 30 000 | 0.5 | G12D (hetero) | NA |
| **PDAC088T** | 40 000 | 0.5 | G12V (hetero) | NA |
| **PDAC089T** | 50 000 | 1 | G12D (hetero) | NA |
| **KPC luc2** | 30 000 | 1 | G12D (hetero) | Mut |

**Supplementary Table 2 (related to Figure 3B and Supplementary Figure 5A).** Pathways enriched in the high OXPHOS PDAC patients (PDAC027T, PDAC074T, PDAC084T) compared to low OXPHOS PDAC patients (PDAC022T, PDAC032T, PDAC085T).

| Reactome Pathways | Proteins | FDR |
|---|---|---|
| Mitochondrial translation initiation_Homo sapiens_R-HSA-5368286 | MRPL12, MRPS26, MRPL40, MRPL46, ICT1, MRPS34, MRPL38, MRPL43, MRPS7, GADD45GIP1, MRPL11, MRPL42, MRPS11, MRPS23, MRPL20, MRPL16, MRPL51, MRPS5, MRPS15, MRPS33, CHCHD1, AURKAIP1, MRPL27, MRPL17, MRPS16, PTCD3, MRPL10, MTFMT, MRPL34, MRPS25, MTIF2, MRPS28, MRPS24, MRPL54, MRPL37, MRPL39, MRPL9, MRPL52, MRPL36, MRPL53, MRPS9, MRPL18, MRPS12, MRPL28, MRPL23, MRPL21, MRPL35 | 0.02851 |
| Mitochondrial translation_Homo sapiens_R-HSA-5368287 | MRPL12, MRPS26, MRPL40, MRPL46, ICT1, MRPS34, MRPL38, MRPL43, MRPS7, GADD45GIP1, MRPL11, MRPL42, MRPS11, MRPS23, MRPL20, MRPL16, MRPL51, MRPS5, MRPS15, MRPS33, CHCHD1, AURKAIP1, TSFM, MRPL27, MRPL17, MRPS16, PTCD3, MRPL10, MTFMT, MRPL34, MRPS25, MTIF2, MTRF1L, MRPS28, MRPS24, MRPL54, TUFM, MRPL37, MRPL39, MRPL9, MRPL52, MRPL36, MRPL53, MRPS9, MRPL18, MRPS12, MRPL28, MRPL23, MRPL21, MRPL35 | 0.02851 |
| Mitochondrial translation termination_Homo sapiens_R-HSA-5419276 | MRPL12, MRPS26, MRPL40, MRPL46, ICT1, MRPS34, MRPL38, MRPL43, MRPS7, GADD45GIP1, MRPL11, MRPL42, MRPS11, MRPS23, MRPL20, MRPL16, MRPL51, MRPS5, MRPS15, MRPS33, CHCHD1, AURKAIP1, MRPL27, MRPL17, MRPS16, PTCD3, MRPL10, MRPL34, MRPS25, MTRF1L, MRPS28, MRPS24, MRPL54, MRPL37, MRPL39, MRPL9, MRPL52, MRPL36, MRPL53, MRPS9, MRPL18, MRPS12, MRPL28, MRPL23, MRPL21, MRPL35 | 0.02851 |
| Mitochondrial translation elongation_Homo sapiens_R-HSA-5389840 | MRPL12, MRPS26, MRPL40, MRPL46, ICT1, MRPS34, MRPL38, MRPL43, MRPS7, GADD45GIP1, MRPL11, MRPL42, MRPS11, MRPS23, MRPL20, MRPL16, MRPL51, MRPS5, MRPS15, MRPS33, CHCHD1, AURKAIP1, TSFM, MRPL27, MRPL17, MRPS16, PTCD3, MRPL10, MRPL34, MRPS25, MRPS28, MRPS24, MRPL54, TUFM, MRPL37, MRPL39, MRPL9, MRPL52, MRPL36, MRPL53, MRPS9, MRPL18, MRPS12, MRPL28, MRPL23, MRPL21, MRPL35 | 0.02851 |
| Respiratory electron transport, ATP synthesis by | UCP1, SLC25A27, NDUFA12, ATP5I, COX6A1, NDUFB9, UQCR10, ECSIT, ATP5G2, NDUFAF3, COX5A, COX14, NDUFV2, SCO2, ATP5H, NDUFB8, | 0.02851 |

| | | |
|---|---|---|
| chemiosmotic coupling, and heat production by uncoupling proteins._Homo sapiens_R-HSA-163200 | NDUFS5, NDUFA7, TACO1, NDUFAF5, NDUFA9, NDUFAB1, ATP5D, NDUFA13, ATP5E, NDUFS3, NDUFAF1, COX6B1, COX4I1, NUBPL, NDUFB10, NDUFC2, COX7A2L, COX16, NDUFA11, ATP5G3, UQCR11, ATP5C1, NDUFB7, TIMMDC1, UCP2, NDUFB6, UQCRH, ETFA, NDUFC1, COX11, COX5B, NDUFS8, NDUFAF7, UQCRC1, COX8A, COX6C, NDUFA10, ETFDH, COX18, UQCRB, ATP5J, NDUFA1 | |
| Complex I biogenesis_Homo sapiens_R-HSA-6799198 | NDUFA12, NDUFB9, ECSIT, NDUFAF3, NDUFV2, NDUFB8, NDUFS5, NDUFA7, NDUFAF5, NDUFA9, NDUFAB1, NDUFA13, NDUFS3, NDUFAF1, NUBPL, NDUFB10, NDUFC2, NDUFA11, NDUFB7, TIMMDC1, NDUFB6, NDUFC1, NDUFS8, NDUFAF7, NDUFA10 | 0.04947 |
| **GO Biological Process Term** | **Proteins** | **FDR** |
| mitochondrial translational elongation (GO:0070125) | MRPL12, MRPS26, MRPL40, MRPL46, MRPS34, MRPL38, MRPL43, MRPS7, GADD45GIP1, LARS2, MRPL11, MRPL42, MRPS11, MRPS23, NDUFA7, MRPL20, MRPL16, MRPL51, ERAL1, MRPS5, MRPS15, GATC, MRPS33, CHCHD1, PTRH1, AURKAIP1, TSFM, MRPL27, MRPL17, MRPS16, PTCD3, EEF1B2, MRPL10, NOA1, MRPL34, MRPS25, EEF2K, MRPS28, MRPS24, MRPL54, TUFM, MRPL37, MRPL39, MRPL9, MRPL52, MRPL36, MRPL53, MRPS9, MRPL18, MRPS12, MRPS2, MRPL28, MRPL23, MRPL21, MRPL35 | 0.02243 |
| mitochondrial translational termination (GO:0070126) | MRPL12, MRPS26, MRPL40, MRPL46, MRPS34, MRPL38, MRPL43, MRPS7, GADD45GIP1, LARS2, MRPL11, MRPL42, MRPS11, MRPS23, NDUFA7, MRPL20, MRPL16, MRPL51, ERAL1, MRPS5, MRPS15, GATC, MRPS33, CHCHD1, PTRH1, AURKAIP1, MRPL27, MRPL17, TRMT112, MRPS16, PTCD3, MRPL10, NOA1, MRPL34, MRPS25, N6AMT1, MTRF1L, MRPS28, MRPS24, MRPL54, MRPL37, APEH, MRPL39, MRPL9, MRPL52, MRPL36, MRPL53, MRPS9, MRPL18, MRPS12, MRPS2, MRPL28, MRPL23, MRPL21, MRPL35 | 0.02718 |
| **GO Cell** | **Proteins** | **P value** |
| mitochondrial respiratory chain complex I, membrane segment (GO:0042653) | NDUFA12, NDUFB9, NDUFV2, NDUFB8, NDUFS5, NDUFA7, SNCA, MT-ND2, NDUFA9, NDUFAB1, NDUFA13, NDUFS3, NDUFAF1, NDUFB10, MT-ND1, MT-ND5, NDUFC2, NDUFA11, NDUFB7, NDUFB6, NDUFC1, NDUFS8, NDUFA10, MT-ND3, NDUFA1, PARK7, FOXRED1 | 0.00739 |

| | | |
|---|---|---|
| mitochondrial respiratory chain complex I, peripheral segment (GO:0042652) | NDUFA12, NDUFB9, NDUFV2, NDUFB8, NDUFS5, NDUFA7, SNCA, MT-ND2, NDUFA9, NDUFAB1, NDUFA13, NDUFS3, NDUFAF1, NDUFB10, MT-ND1, MT-ND5, NDUFC2, NDUFA11, NDUFB7, NDUFB6, NDUFC1, NDUFS8, NDUFA10, MT-ND3, NDUFA1, PARK7, FOXRED1 | 0.00739 |
| mitochondrial respiratory chain complex I (GO:0005747) | NDUFA12, NDUFB9, NDUFV2, NDUFB8, NDUFS5, NDUFA7, SNCA, MT-ND2, NDUFA9, NDUFAB1, NDUFA13, NDUFS3, NDUFAF1, NDUFB10, MT-ND1, MT-ND5, NDUFC2, NDUFA11, NDUFB7, NDUFB6, NDUFC1, NDUFS8, NDUFA10, MT-ND3, NDUFA1, PARK7, FOXRED1 | 0.00739 |
| mitochondrial large ribosomal subunit (GO:0005762) | MRPL12, MRPL40, MRPL46, MRPL38, MRPL43, MRPL11, MRPL42, MPV17L2, MRPL20, MRPL16, MRPL51, MRPL27, MRPL17, MRPL10, MRPL34, MRPL54, MRPL37, MRPL39, MRPL9, MRPL52, MRPL36, MRPL53, MRPL18, MRPL28, MRPL23, MRPL21, MRPL35, MRPL48 | 0.00747 |